Title

Hanging droplets from liquid surfaces

Journal

Proceedings of the National Academy of Sciences of the United States of America, 117(15)

ISSN

0027-8424

Authors

Xie, Ganhua

Forth, Joe

Zhu, Shipei

et al.

Publication Date

2020-04-14

DOI

10.1073/pnas.1922045117

Peer reviewed

Hanging droplets from liquid surfaces

Ganhua Xie[a,b], Joe Forth[a,c], Shipei Zhu[d], Brett A. Helms[e], Paul D. Ashby[e], Ho Cheung Shum[d], and Thomas P. Russell[a,b,f,g,1]

[a] Materials Sciences Division, Lawrence Berkeley National Laboratory, Berkeley, CA 94720; [b] Polymer Science and Engineering Department, University of Massachusetts, Amherst, MA 01003; [c] Department of Chemistry, University College London, London WC1H 0AJ, United Kingdom; [d] Department of Mechanical Engineering, The University of Hong Kong, Hong Kong SAR, China; [e] The Molecular Foundry, Lawrence Berkeley National Laboratory, Berkeley, CA 94720; [f] Beijing Advanced Innovation Center for Soft Matter Science and Engineering, Beijing University of Chemical Technology, Beijing 100029, China; and [g] Advanced Institute for Materials Research, Tohoku University, Sendai 980-8577, Japan

Natural and man-made robotic systems use the interfacial tension between two fluids to support dense objects on liquid surfaces. Here, we show that coacervate-encased droplets of an aqueous polymer solution can be hung from the surface of a less dense aqueous polymer solution using surface tension. The forces acting on and the shapes of the hanging droplets can be controlled. Sacs with homogeneous and heterogeneous surfaces are hung from the surface and, by capillary forces, form well-ordered arrays. Locomotion and rotation can be achieved by embedding magnetic microparticles within the assemblies. Direct contact of the droplet with air enables in situ manipulation and compartmentalized cas- cading chemical reactions with selective transport. Applications including functional microreactors, motors, and biomimetic robots are evident.

compartmentalization | hanging droplets | biomimetic | aqueous two-phase system | droplet transport

Nature harnesses surface tension to support dense objects on liquid surfaces (1–3). Water striders (4–7), beetle larvae (8), and mosquito larvae (9) harness surface tension to stand, walk, jump, or hang on the surface of water for mating, predation, escape, and survival. These natural phenomena have inspired research into producing man-made robotic systems for trans- port across water, which may find potential applications in drug delivery, fluid m ixing, a nd p umping (6, 1 0–14). W hether natu- ral or man-made, these systems consist of a hydrophobic body in contact with water, where the interface between these two systems is characterized by large interfacial tensions that pre- vent the hydrophobic body from breaking through the surface and sinking. Here, we present a study on two immiscible aque- ous solutions (15) containing oppositely charged polyelectrolytes where droplets of the denser solution bounce on the surface, like water striders, form a membrane that can hang droplets from the water surface, like mosquito larvae, or form a shroud that com- pletely wraps the denser fluid as it sinks. The density difference between the solutions is balanced by surface tension forces, while the size of the droplets that can be hung from the air–water inter- face is determined by the polyelectrolyte coacervate that forms upon droplet impact (16–18). The magnitude of the interfacial forces acting on the droplet and the shapes of the droplets can be controlled by the droplet momentum at impact and the poly- electrolyte concentrations. Vertically and horizontally structured coacervate sacs with homogeneous and heterogeneous surfaces can be produced that hang from the surface and, due to cap- illary forces (19, 20), form well-ordered arrays. Controllable locomotion and rotation on the surface are also achieved by functionalizing the hanging droplets with magnetic microparti- cles (MMPs). The suspended droplets are in direct contact with air, enabling in situ manipulation of the droplets and using the encapsulated aqueous phases for compartmentalized cascading chemical reactions with selective transport.

Results

We studied the now-classic (21–24), aqueous two- phase sys- tem (ATPS) of a dextran solution containing polycations and a

poly(ethylene glycol) (PEG) solution containing polyanions as an example, although the results are general for other ATPSs. The immiscible aqueous polymer solutions have ultralow interfa- cial tensions of 10^{-7} N m^{-1} to 10^{-4} N m^{-1}, depending on PEG and dextran concentrations. A droplet of an aqueous dextran solution containing poly(diallyl dimethylammonium chloride) (PDADMAC), a polycation, with a density ρ_{Dex} = 1.055 g mL^{-1} and droplet diameters D = 2.48 mm to 4.03 mm, was released from different heights h = 5 mm to 60 mm onto an aque- ous PEG solution with a lower density (ρ_{PEG} = 1.014 g mL^{-1}) containing poly(sodium 4-styrenesulfonate) (PSS), a polyanion, as shown in Fig. 1*A*. When the two aqueous phases come into contact with one another, the oppositely charged polyelec- trolytes form a coacervate at the interface. Surprisingly, rather
than sinking, the denser dextran droplet is arrested at the sur- face by the coacervate and hangs from the air–liquid interface (Fig. 1*B* and Movie S1). Absent polyelectrolytes (Movie S2), the dextran droplet of the same volume penetrates the surface and sinks.

We investigated the origins of this behavior by using a high- speed camera to record the falling droplet. As shown in Fig. 1*B* and Movies S3–S5, the droplets experience three stages after release from a height h = 5 mm: impact, bouncing, and hanging. At the initial impact stage, the droplet thins an air layer between the droplet and surface of the solution, but there is no liquid– liquid contact, and the droplet recoils from the surface (25–27). After bouncing away, the droplet returns to and rests on the surface, and the air layer continually thins until the two aque- ous phases establish contact and the droplet begins to spread on the surface (26). Concurrently, a polyelectrolyte coacervate

Significance

Heavier objects usually sink in a less dense fluid. Water- walking anthropods and biomimetic water-walking robots harness surface tension in order to overcome this tendency, floating on top of liquids. By hanging a coacervate-encased droplet of a denser aqueous dextran solution from the sur- face of an aqueous solution of poly(ethylene glycol) (PEG), we harness the binding of dense droplets to interfaces by surface tension to build two-dimensional ensembles of structurally complex droplets. Applications ranging from reaction vessels with selective transport to motors and robotics are

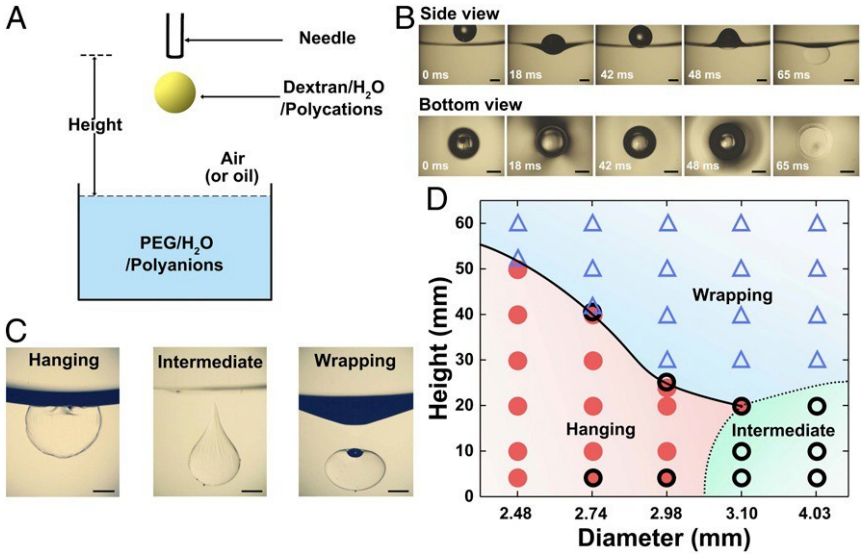

Fig. 1. Hanging a structured droplet on the interface between a less dense liquid and air (or oil). (*A*) Schematic of the experiment. A drop of dextran solution containing polycations falls into a PEG solution containing polyanions of lower density. The release height (*h*) and size of the droplet are controlled by the position and droplet diameter of the needle. (*B*) Sequence of events observed from the side (*Top*) and bottom (*Bottom*) in a typical experiment where a dextran droplet hangs on the surface of the PEG solution. Here, h = 5 mm, and diameter D = 2.98 mm. (Scale bars, 1 mm.) (*C*) Three typical droplet states after falling from the needle tip: hanging, intermediate, and wrapping. (Scale bars, 1 mm.) (*D*) State diagram as a function of *h* and *D*: hanging (red filled circles), intermediate (black open circles), and wrapping (blue open triangles). Lines (solid and dashed) indicate the observed thresholds between the different states.

forms at the interface between the two aqueous phases. Since the droplet has a higher density, gravity causes it to sink, but surface tension at the edges of the coacervate layer resists the sinking. Sinking continues until surface tension and buoyancy forces are balanced, and the droplet hangs in a coacervate sac. Increas- ing the release height of the droplet increases the momentum of the droplet at contact, forcing the droplet deeper into the PEG solution. Above a critical release height, the droplet tem- porarily hangs, but then is enveloped by the coacervate and sinks (Fig. 1*C* and Movie S6) (28). At even higher droplet release heights, the droplet penetrates the interface with an air bub- ble at the top, as the encapsulated droplet sinks (Movie S7) (29). Fig. 1*D* summarizes the fate of the dextran (15 wt %)/ PDADMAC (0.8 wt %) droplets falling onto a pool of PEG (10 wt %)/PSS (1 wt %) as a function of the release height and droplet diameter. The threshold height for hanging (black solid line) decreases with increasing droplet diameter. When the droplet diameter, *D*, exceeded 3.1 mm, no hanging of the droplet was observed, regardless of release height. We then studied the effects of placing a layer of oil (silicone oil, $\rho_1 = 0.996$ g mL−1) atop the PEG solution. This does not prevent the droplet from hanging (*SI Appendix*, Fig. S1*B*). By increasing the oil density $\rho_2 = 1.040$ g mL−1, a density greater than the PEG solution, the droplet still hangs at the water–oil interface (*SI Appendix*, Fig. S1*C*).

To clarify the role of the coacervate, we then studied aqueous polymer solutions that contained no polyelectrolyte. Absent the polyelectrolytes, the largest dextran droplets that could be sus- pended from the air–liquid interface were 0.13 μL (*SI Appendix*, Fig. S2) (30, 31), over two orders of magnitude smaller than the droplets studied in Fig. 1. When studying ensembles of 0.13-μL droplets, the droplets coalesced, and the larger droplet sub- sequently sunk. Clearly, the polyelectrolyte coacervate formed when the two aqueous phases contact one another is critical both in preventing droplet coalescence and in defining the size of the droplet that can be suspended. As such, the rate at which the coacervate forms relative to the droplet penetration into the PEG solution is central to the hanging of the dextran droplet.

If the polyelectrolyte concentration is too low, or the release height is too high, the coacervate does not support hanging of the droplet (*SI Appendix*, Fig. S3). Increasing the polyelec- trolyte concentration leads to more rapid coacervate formation and a higher threshold height, h^*. For the remainder of this study, unless stated otherwise, the concentrations of PSS and PDADMAC are 1 wt % and 0.8 wt %, respectively. We note that other polyelectrolytes and ion-cross-linked hydrogel systems (Movie S8 and *SI Appendix*, Tables S1 and S2) yield similar results, underscoring the generality of our findings. The concen- trations of dextran and PEG were also varied to tune the density difference ($\Delta\rho$) (*SI Appendix*, Fig. S4 and Table S3). Intuitively, increasing $\Delta\rho$ led to h^* decreasing. Consequently, the concen- trations of dextran and PEG were fixed at 15 wt % and 10 wt %, respectively, unless stated otherwise.

We then quantitatively investigated the conditions for suc- cessful hanging of the droplets. Shown in Fig. 2 *A* and *B* are side and top views of hanging droplets, and the stresses acting on the system are shown in Fig. 2*C*. The level of the dextran solution is lower than that of the PEG, and the edge of the coacervate is below the surface levels of both solutions. This was also confirmed by confocal microscopy images (*SI Appendix*, Fig. S5). The presence of the solid coacervate means there are two relevant three-phase contact lines (TPCLs) to consider; the PEG–air–coacervate TPCL and the dextran–air–coacervate TPCL. Somewhat counterintuitively, the condition for hanging the dextran droplet from the air–PEG interface is determined solely by a force balance between gravitational stresses and sur- face stresses on the PEG side of the droplet (simply put, the dextran droplet cannot lift itself up). Neglecting air–coacervate surface tension, the surface stresses acting on the TPCLs in this system itself are therefore given by two Young equations,

$$\gamma_{CP}\sin\beta + \frac{F}{G}_{C} = \gamma_{PEG}\sin\alpha \quad \textbf{[1]}$$

$$\gamma_{CD}\sin\beta = \gamma_{Dex}\sin\phi, \quad \textbf{[2]}$$

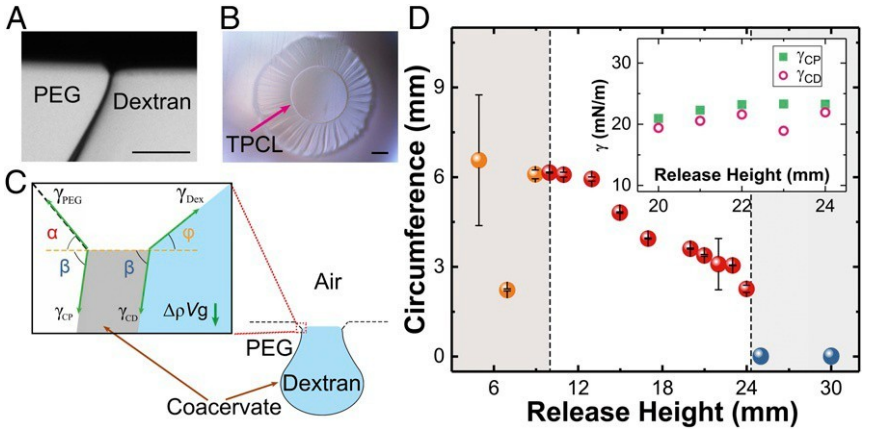

Fig. 2. Mechanism analysis for the hanging droplet. (*A*) Side view and (*B*) top view of the TPCL of the hanging droplet. (Scale bars, 0.3 mm.) (*C*) Sketch of the effect of surface tension and gravity on the hanging dextran droplet. The surface tension from PEG solutions (γ_{PEG}) pulls on the droplet balancing gravity force ($\Delta\rho$Vg) and interfacial tension between the coacervate and PEG solution (γ_{CP}). For simplicity, the surface tension between the coacervate and air is not shown. (*D*) The circumference of the TPCL as a function of the release height (*h*). Orange dots mark unstable TPCL, darker red dots mark stable TPCL, and blue dots mark no TPCL. (*Inset*) The calculated value of γ_{CP} and interfacial tension between the coacervate and dextran solution (γ_{CD}) at different dropping heights.

where γ_{PEG}, γ_{Dex}, γ_{CP} , and γ_{CD} are the air–PEG, air–dextran, coacervate–PEG, and coacervate–dextran surface ten- sions, respectively. α, β, and ϕ are the contact angles defined in Fig. 2*C*, and *C* is the length of the TPCL. Both the length and the shape of the TPCL are determined by the coacervate (Fig. 2*D* and *SI Appendix*, Fig. S6). The elastic polyelectrolyte–polyelectrolyte coacervate formed at the PEG–dextran interface gives rise to anisotropic surface stresses. The effect of this can be seen in both the wrinkling of the PEG–dextran interface in the immersed droplet and the shape of the TPCL (Fig. 2*B* and *SI Appendix*, Figs. S6 and S7). We note that there is a possible enhancement of the vertical force that surface tension can pro- vide due to the wrinkling. When $h < 10$ mm, the TPCL has an irregular polygonal shape. After bouncing, fluctuations along the thinning layer of air separating the droplet and the surface enable off-axis contact, and a nonsymmetric TPCL (Movie S3) forms. Higher release heights of the droplet reduce the formation time of the coacervate, reducing the amount of material formed dur- ing impact, as well as changing the shape of the TPCL. For $\approx$ 10 mm $< h <$ 24.5 mm, the TPCL is roughly circular in shape, and C $2\pi r$. By measuring α, β, and ϕ, the surface tensions of the aqueous phases against the coacervate can be directly mea- sured (Fig. 2 *D*, *Inset*). Both surface tensions are invariant with release height, as would be expected for material parameters;
γ_{CP} was calculated to be 22 $\pm$ 61 1.03 mN m−1, close to the cal- culated interfacial tension between the coacervate and dextran solution (γ_{CD}) of 20.49 $\pm$ 1.31 mN m−1 (*Materials and Methods*, Fig. 2 *D*, *Inset* and *SI Appendix*, Table S4). We note that there is a small variation in the measured values of γ_{CP} and γ_{CD} , which we attribute to slight noncircularities in the TPCL, while the values of these interfacial tensions are similar in magnitude to reported interfacial tensions of hydrogels (32), a reasonable comparative case.

The structure of the hanging droplet was varied by translat- ing the point where successive droplets impinged on the surface (horizontal stacking) (*SI Appendix*, Fig. S8*A* and Movie S9) or letting successive droplets impinge on the surface at the same point (vertical stacking) (*SI Appendix*, Fig. S8*B* and Movie S10). Due to the large variety of polyelectrolytes, functional hanging droplets and hanging droplets with heterogeneous sur- faces are easily produced, as shown in Fig. 3. Janus droplets, for example, were prepared by using two different polycations [poly(allylamine hydrochloride) (PAH) and chitosan] (Fig. 3*A*). The heterogeneous nature of the surface was confirmed by con-

focal microscopy (*SI Appendix*, Fig. S9). By controlling the lateral point of droplet impingement, structures ranging from clover- leafs (Fig. 3*B*) to hearts, dumbbells, necklaces (*SI Appendix*, Fig. S10 *A*–*D*), or segmented constructs (Fig. 3*C* and *SI Appendix*, Fig. S10 *E*–*G*) are easily produced. Droplets sequentially imping- ing on the surface at the same contact point produce an encapsulant having walls comprising different coacervates (segmented walls) (Fig. 3 *D* and *E* and *SI Appendix*, Fig. S10*H*). These strategies can be combined to generate encapsulants with more complex structures, as shown in *SI Appendix*, Figs. S8*C*, S10*I*, and S11. Consequently, hanging structured droplets with heterogeneous surfaces, cornerstones for the develop- ment of aqueous-based micromotors and microrobots, are easily produced.

Fig. 4*A* shows the collective behavior of ensembles of hanging droplets. When the droplets are randomly hung on the sur- face, capillary forces draw the hanging droplets to each other, leading to the formation of ordered arrays (Movie S11). When MMPs are mixed into hanging droplets, MMPs impart magnetic properties to the droplets so that the droplets hanging from the surface can be manipulated with an external mag- netic field (Fig. 4 *B*–*D* and Movie S12), making aggregation reversible. In addition, in a rotating magnetic field, the hang- ing droplet rotates to follow the field (Fig. 4*E* and Movie S13) (33). This suggests that the magnetic particles are imbedded and fixed in the coacervate layer (21); otherwise, the particles would rotate independently, and the coacervate would remain stationary. These dimensionally confined ensembles of magnetic droplets offer compelling possibilities for future work in investigating their collective behavior in the presence of an external magnetic field (14).

Selective ion diffusion between the hanging droplets and the bulk solution was also observed (23, 34), as shown in Fig. 4*F* and *SI Appendix*, Fig. S12. This enables selective exchange of reagents and reactants between the compartmentalized hanging droplets (*SI Appendix*, Fig. S13) that exploit the interconnectiv- ity of two aqueous phases with a surrounding gas phase. As an example, we hung two droplets next to each other (Fig. 4*G*). One of these droplets contained glucose oxidase (GOx), which was shown to react with oxygen from the surrounding air, after absorbing glucose from the bulk PEG phase. The hydrogen peroxide produced then diffused into a neighboring droplet to feed horseradish peroxidase (HRP)-catalyzed *o*-dianisidine oxi- dation (Fig. 4*G*). As shown in Fig. 4 *H*–*J*, the light brown

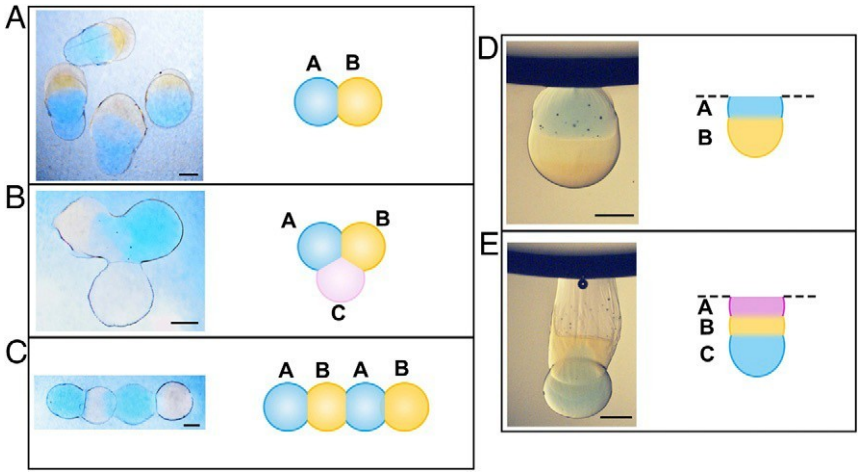

Fig. 3. Segmented hanging droplets with heterogeneous surface. (*A*–*C*) Microscopic (*Left*) and schematic (*Right*) images of the horizontally stacked droplets with heterogeneous surfaces viewed from the top. (*A*) Janus droplets. (*B*) Cloverleaf-shaped droplets. (*C*) Horizontally segmented tubules fabricated in a similar manner. (*D* and *E*) Microscopic (*Left*) and schematic (*Right*) images of the vertically stacked droplets with heterogeneous surfaces from the side view. (*D*) Janus droplets. (*E*) Vertically segmented droplets. The blue solution contains Cy5-labeled PEI, the yellow solution contains FITC-labeled PAH, the light red solution contains rhodamine-labeled chitosan, and the colorless solution contains PDADMAC. (Scale bars, 1 mm.)

o-dianisidine–containing droplet turns dark purple due to the presence of the oxidation product. The comparative ease with which these multistep, compartmentalized reaction cascades can be engineered suggests the potential to engineer higher-order emergent behavior via chemical feedback loops (35).

Conclusions

A simple route to hang droplets of an aqueous polymer solu- tion from the surface of a second aqueous polymer solution is shown. These hanging droplets are bound to the air–water interface by capillary forces acting on the TPCL, the length of which is determined by polyelectrolyte complex. These droplets can be easily produced with homogeneous or heterogeneous surfaces, and self-assemble into well-ordered arrays due to capil- lary forces. Furthermore, they can be functionalized, for exam- ple with MMPs, to control the locomotion of the droplets, and, due to the nature of the assemblies, can selectively trans-port chemicals from one droplet to another or be used as encapsulated reaction vessels, where reactions rely on direct contact with air. These hanging droplets have potential applica- tions in functional microreactors, micromotors, and biomimetic microrobots.

Materials and Methods

Fabrication of Hanging Droplets. Dextran droplets containing polycations were injected from a syringe, whose height and injecting rate were com- puter controlled. Needles of different sizes connected to the syringe were used to control the diameters of the droplets. The PEG solution contain-

ing polyanions was carefully placed into a cuvette (12.5 mm × 12.5 mm × 45 mm) made of polystyrene. The various samples of different dex-

tran, PEG, polycations, and polyanions concentrations are summarized in Fig. 1*D* and *SI Appendix*, Figs. S3 and S4. To obtain fluorescent images of the hanging droplet, fluorescein i sothiocyanate (FITC)-labeled dextran and methoxy-PEG (mPEG)-Rhodamine were used. Ten wt % PEG solu- tion containing 1 wt % PSS and a trace amount of anthracene-labeled poly(methacrylic acid) and mPEG-Rhodamine were placed into a tissue culture dish (35 mm × 10 mm, polystyrene, from Falcon). A droplet of

For horizontal, after droplet A was hung on the PEG surface, the needle was moved laterally from its original position by a predetermined distance (of order several millimeters), and droplet B was released from the needle, partially covering droplet A, as shown in *SI Appendix*, Fig. S8*A*. By chang- ing the material in the droplet, a Janus droplet can be obtained as shown in Fig. 3*A*. By changing the contents of subsequent drops after horizon- tal displacement, a heterogeneous array of connected droplets could be obtained. For vertical, after droplet A was hung from the PEG surface, with- out changing the lateral position of the needle, droplet B was released and let fall onto the droplet hanging from the surface, as shown in *SI Appendix*, Fig. S8*B*. Multiple droplets of either the same or different chemical com- positions can be sequentially deposited in this manner (*SI Appendix*, Fig. S8*C*). If the droplet volumes are changed, mosaic patterns can be produced, or larger sacs hanging from the surface with a sequenced heterogeneity. Whether the vertically stacked droplets hang from the surface is dictated by the surface tension of the coacervate formed by the last drop. A wide array of horizontally and vertically patterned construct can be produced in this manner (SI *Appendix*, Fig. S10). More-complex structures can be produced by combining the vertical and horizontal stacking strategies, as shown in *SI Appendix*, Figs. S8*C* and S11. For horizontally stacked droplets, the shell of these dextran droplets remains sectioned, but the droplet shape changes to minimize the surface area, constrained by the coacervate (*SI Appendix*, Fig. S14). For vertically stacked droplets, the shape of the dextran droplets is preserved, and the surface of the droplets remains sectioned for hours (*SI Appendix*, Fig. S15). In our experiments, we used four polycations (PDADMAC, chitosan, polyethylenimine [PEI], and PAH) and PSS to fabri-cate heterogeneous surfaces as proofs of concept. To make the observation of these heterogeneous surfaces easier to see, dye-labeled polycations (Cy3- labeled PDADMAC [pink], rhodamine-labeled chitosan [red], Cy5-labeled PEI [blue], and FITC-labeled PAH [yellow]) were mixed into the dextran phase.

Selective Ion Separation. Before hanging the dextran droplet, 1.36 µM Nile

15 wt % dextran solution containing 0.8 wt % PDADMAC and a trace amount of FITC-labeled dextran was let fall into the PEG solution from a height of 15 mm. After the hanging droplet became stable on the surface of PEG solution, fluorescent i mages w ere t aken a s s hown i n *SI Appendix*, Fig. S5.

Droplet Stacking on the Surface of PEG Solution. Two different routes (hor- izontal and vertical) were used to place multiple droplets at the interface.

blue A (NBA) and 250 μM fluorescein sodium salt were dissolved in the
dextran phase. The dye-mixed dextran droplets were then hung from the surface of the PEG solution. After 30 min, we observed obvious ion sep- aration between the droplet and the PEG phase as NBA diffused out of the droplet and fluorescein stayed in the sac, in agreement with previous reports (*SI Appendix*, Fig. S12) (23, 34). When another droplet without dyes was hung adjacent to it, fluorescein was observed in its neighbor, and NBA was not observed, which means fluorescein molecules are able to diffuse between droplets as shown in *SI Appendix*, Fig. S13.

Aggregation Behavior of the Hanging Droplets. Dextran droplets were ran- domly hung on the surface of PEG solution. Around the edge of the sac hanging from the surface, the PEG solution showed a noticeable downward curvature due to the gravitation forces acting on the sac. Consequently, capillary forces exerted an attractive interaction between the hanging sacs

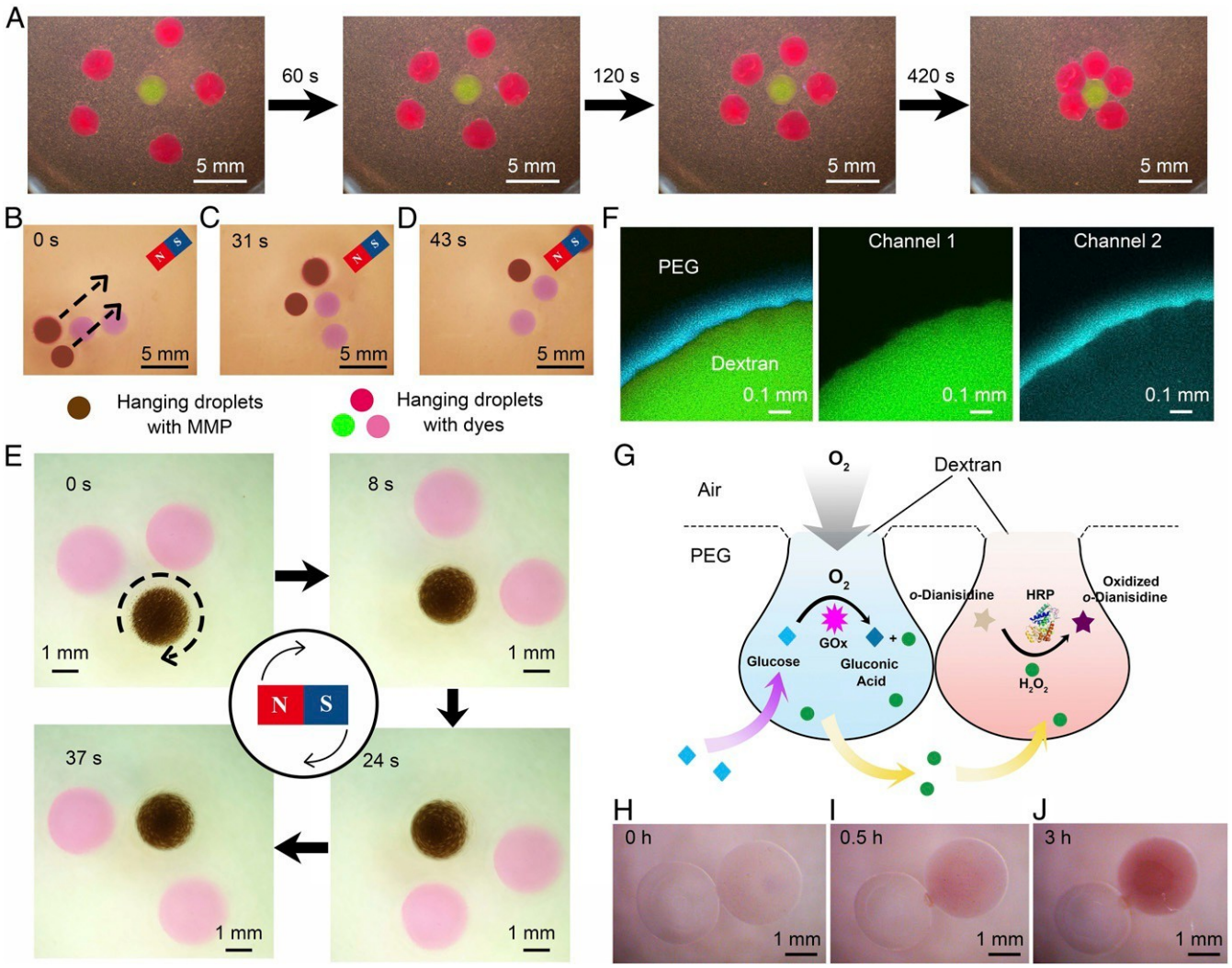

Fig. 4. Locomotion and compartmentalized reaction by bioinspired structured droplets hanging on a liquid surface. (*A*) Capillary force-induced aggregation of hanging droplets. Randomly placed hanging droplets are drawn to each other and to the center of the PEG solution surface over 420 s. (*B–D*) Time evolution of magnetic field-controlled locomotion of hanging droplets on the surface. When modified with MMPs, the hanging droplets can be moved across the surface with an external magnetic field. (*E*) Three hanging droplets with one containing MMPs in a rotating magnetic field. (*F*) Images of ion separation between the hanging droplet and PEG solution by confocal microscopy. Blue is NBA, and green is fluorescein. (*G*) Schematic of the bioinspired hanging microreactor system. A hanging droplet absorbs glucose from the PEG solution and takes in oxygen from the air to oxidize the glucose. The hydrogen peroxide produced diffuses into and fuels the reaction in the neighboring hanging droplet. (*H–J*) Time evolution of the bioinspired hanging microreactor system. The *o*-dianisidine–mixed droplet (light brown, right) gradually turns dark purple.

(19). The sacs are seen to aggregate over hundreds of seconds (Fig. 4*A* and Movie S11). To make the aggregation behavior easier to examine, dyes were mixed into the dextran droplet. The green droplet contains fluorescein, a nd t he r ed o ne c ontains s ulforhodamine B s odium s alt. All of these dyes will stay in the droplets, due to the electrostatic attraction by PDADMAC in the dextran phase and electrostatic repulsion by PSS in the PEG phase.

Controllable Locomotion of the MMP-Functionalized Hanging Droplets under Magnetic Field. Amino-functionalized MMP solution (40 mg mL^{-1} to 55 mg mL^{-1}) was mixed into the dextran phase containing 1.4 wt % PDADMAC with volume ratio 1:10. After hanging on the surface of the PEG solution containing 1.5 wt % PSS, MMP-functionalized droplets exhibit controllable locomoting and rotating on the surface by following the mag- netic field. W ithout M MPs, t his d oes n ot o ccur (Movies S 12 a nd S 13). We used a commercial horseshoe magnet with a measured magnetic strength of 100 mT/μ_0 at the magnet. At a distance of 1.7 cm, the field strength decreased to 30 mT/μ_0, and, at 3.5 cm, the magnetic field strength decreased to 8 mT/μ_0. During the experiments, the droplets were 1.5 cm from the magnet.

Fabrication of Hanging Microreactors. The hanging droplet was composed of 2 wt % PSS, 1 mg mL^{-1} GOx, and 15 wt % dextran; 1 mg mL^{-1} D-glucose was mixed into the PEG phase (10 wt %) containing 0.91 wt % PAH. As shown in Fig. 4*G*, the hanging droplet is able to absorb D-glucose from the PEG solution and takes in oxygen from the air to oxidize D-glucose into hydrogen peroxide and gluconic acid catalyzed by GOx. When another dex- tran droplet composed of 5 mg mL^{-1} *o*-dianisidine and 11 mg mL^{-1} HRP was hung next to the droplet hanging from the surface, hydrogen peroxide diffused into the new droplet and fed the *o*-dianisidine oxidation catalyzed by HRP. Therefore, light brown from *o*-dianisidine in the dextran phase turns into dark purple from the oxidized products as shown in Fig. 4 *H–J*.

Estimation of the Interfacial Tensions γ_{CP} and γ_{CD}. When taking the dextran droplet and the coacervate as one object, we can know that the condition for hanging the dextran droplet from the air–PEG interface is determined solely by a force balance between gravitational stresses and surface stresses on the PEG side of the droplet (Fig. 2*C*). Therefore, we can obtain Eq. **1**. Meanwhile, when we analyze the force balance of the coacervate, it is nec-

essary to note here that, in the aqueous phase, there are, in fact, two distinct surface tensions related to the coacervate, the surface tension between the

PEG-rich aqueous phase and the coacervate, γ_{CP} , and the surface tension between the dextran-rich aqueous phase and the coacervate, γ_{CD} (Fig. 2*C*). If neglecting the thickness of the coacervate, surface stresses acting on the coacervate in this system are given by

$$\gamma_{ws} sin\beta + \frac{F_G}{C} = \gamma_{aw}\,, \qquad [3]$$

where $\gamma_{ws} = \gamma_{CP} \sin\beta + \gamma_{CD} \sin\beta$, and $\gamma_{aw} = \gamma_{PEG} \sin\alpha + \gamma_{Dex} \sin\phi$, with γ_{PEG} and γ_{Dex} being the air–PEG and air–dextran surface tensions, respectively, and α, β, and ϕ defined in Fig. 2*C*. The balance of forces acting on the coacervate is given by

$$(\gamma_{aw} - \gamma_{ws})C = F_G \qquad [4]$$

$$(\gamma_{PEG} sin\alpha + \gamma_{Dex}\, sin\phi - \gamma_{CP}\, sin\beta - \gamma_{CD} sin\beta)C = F_G. \qquad [5]$$

Compared with Eqs. **1** and **5**, we can get Eq. **2**. As γ_{Dex} (26.80 $mN{\cdot}m^{-1}$), β, and ϕ have been measured, we can calculate the value of γ_{CD} to be 20.49 ± 1.31 $mN{\cdot}m^{-1}$ (Fig. 2 *D*, *Inset* and *SI Appendix*, Table S4), which is very close to γ_{CP} . It is important to note the role of the coacervate in determining *C*. In the absence of polyelectrolytes, the TPCL can shrink to zero length with zero energetic cost, and the droplet is pulled through the air–water interface. By contrast, in the presence of the polyelectrolytes, the coacervate forms a ring at the TPCL, whose length determines the magnitude of the force binding the droplet to the air–water interface. As we show above, this length is determined by both the concentration of polyelectrolytes and the amount of time the dextran-rich droplet is in contact with the PEG–air interface before being submerged in the PEG-rich phase.

Data Availability Statement. Access to our underlying data or samples will be granted upon request to the corresponding author. Where feasible, meth- ods and protocol data will be provided upon request through a DROPBOX established for this research.

ACKNOWLEDGMENTS. The design, characterization, and analysis of the hanging droplets experiments were supported by the US Department of Energy, Office of Science, Office of Basic Energy Sciences, Materials Sciences and Engineering Division under Contract DE-AC02-05-CH11231 within Pro- gram KCTR16, Adaptive Interfacial Assemblies Toward Structuring Liquids. Transport and assembly studies were supported by the Army Research Office under Contract W911NF-17-1-0003.

1. J. W. M. Bush, D. L. Hu, Walking on water: Biolocomotion at the interface. *Annu. Rev. Fluid Mech.* **38**, 339–369 (2006).
2. S. Lee, J. W. M. Bush, A. E. Hosoi, E. Lauga, Crawling beneath the free surface: Water snail locomotion. *Phys. Fluids* **20**, 082106 (2008).
3. N. J. Mlot, C. A. Tovey, D. L. Hu, Fire ants self-assemble into waterproof rafts to survive floods. *Proc. Natl. Acad. Sci. U.S.A.* **108**, 7669–7673 (2011).
4. X.-Q. Feng, X. Gao, Z. Wu, L. Jiang, Q.-S. Zheng, Superior water repellency of water strider legs with hierarchical structures: Experiments and analysis. *Langmuir* **23**, 4892– 4896 (2007).
5. X. Gao, L. Jiang, Water-repellent legs of water striders. *Nature* **432**, 36 (2004).
6. J. S. Koh et al., Jumping on water: Surface tension–dominated jumping of water striders and robotic insects. *Science* **349**, 517–521 (2015).
7. Q. Wang, X. Yao, H. Liu, D. Que´ re´ , L. Jiang, Self-removal of condensed water on the legs of water striders. *Proc. Natl. Acad. Sci. U.S.A.* **112**, 9247–9252 (2015).
8. D. L. Hu, J. W. Bush, Meniscus-climbing insects. *Nature* **437**, 733–736 (2005).
9. S. C. Lee, J. H. Kim, S. J. Lee, Floating of the lobes of mosquito (Aedes togoi) larva for respiration. *Sci. Rep.* **7**, 43050 (2017).
10. W. Hu, G. Z. Lum, M. Mastrangeli, M. Sitti, Small-scale soft-bodied robot with multimodal locomotion. *Nature* **554**, 81–85 (2018).
11. J. Jiang *et al.*, Directional pumping of water and oil microdroplets on slippery surface. *Proc. Natl. Acad. Sci. U.S.A.* **116**, 2482–2487 (2019).
12. L. Jiang *et al.*, "Water strider" legs with a self-assembled coating of single-crystalline nanowires of an organic semiconductor. *Adv. Mater.* **22**, 376–379 (2010).
13. X. Liu *et al.*, Bioinspired oil strider floating at the oil/water interface supported by huge superoleophobic force. *ACS Nano.* **6**, 5614–5620 (2012).
14. G. Grosjean, M. Hubert, N. Vandewalle, Magnetocapillary self-assemblies: Locomo- tion and micromanipulation along a liquid interface. *Adv. Colloid. Interface Sci.* **255**, 84–93 (2018).
15. P.-A˚ . Albertsson, Partition of proteins in liquid polymer–polymer two-phase systems. *Nature* **182**, 709–711 (1958).
16. G. Galilei, *Discourse Concerning the Natation of Bodies upon, and Submersion in, the Water* (William Leybourn, London, United Kingdom, 1663).
17. J. B. Keller, Surface tension force on a partly submerged body. *Phys. Fluids* **10**, 3009– 3010 (1998).
18. D. Vella, Floating versus sinking. *Annu. Rev. Fluid Mech.* **47**, 115–135 (2015).
19. D. Vella, L. Mahadevan, The "Cheerios effect."*Am. J. Phys.* **73**, 817–825 (2005).
20. D. Vella, P. D. Metcalfe, R. J. Whittaker, Equilibrium conditions for the floating of multiple interfacial objects. *J. Fluid. Mech.* **549**, 215–224 (2006).
21. S. D. Hann, K. J. Stebe, D. Lee, Awe-somes: All water emulsion bodies with permeable shells and selective compartments. *ACS Appl. Mater. Interfaces* **9**, 25023–25028 (2017).
22. Q. Ma, Y. Song, J. W. Kim, H. S. Choi, H. C. Shum, Affinity partitioning-induced self-assembly in aqueous two-phase systems: Templating for polyelectrolyte micro- capsules. *ACS Macro Lett.* **5**, 666–670 (2016).
23. G. Xie *et al.*, Compartmentalized, all-aqueous flow-through-coordinated reaction systems. *Chem* **5**, 2678–2690 (2019).
24. Y. Liu, R. Lipowsky, R. Dimova, Concentration dependence of the interfacial ten- sion for aqueous two-phase polymer solutions of dextran and polyethylene glycol. *Langmuir* **28**, 3831–3839 (2012).
25. Y. Amarouchene, G. Cristobal, H. Kellay, Noncoalescing drops. *Phys. Rev. Lett.* **87**, 206104 (2001).
26. F. Blanchette, T. P. Bigioni, Partial coalescence of drops at liquid interfaces. *Nat. Phys.* **2**, 254–257 (2006).
27. H. Y. Lo, Y. Liu, L. Xu, Mechanism of contact between a droplet and an atomically smooth substrate. *Phys. Rev. X* **7**, 021036 (2017).
28. R. M. Capito, H. S. Azevedo, Y. S. Velichko, A. Mata, S. I. Stupp, Self-assembly of large and small molecules into hierarchically ordered sacs and membranes. *Science* **319**, 1812–1816 (2008).
29. D. Kumar, J. D. Paulsen, T. P. Russell, N. Menon, Wrapping with a splash: High-speed encapsulation with ultrathin sheets. *Science* **359**, 775–778 (2018).
30. C. M. Phan, B. Allen, L. B. Peters, T. N. Le, M. O. Tade, Can water float on oil? *Langmuir* **28**, 4609–4613 (2012).
31. C. M. Phan, Stability of a floating water droplet on an oil surface. *Langmuir* **30**, 768– 773 (2014).
32. R. N. King, J. D. Andrade, S. M. Ma, D. E. Gregonis, L. R. Brostrom, Interfacial tensions at acrylic hydrogel-water interfaces. *J. Colloid. Interface Sci.* **103**, 62–75 (1985).
33. X. Liu *et al.*, Reconfigurable ferromagnetic liquid droplets. *Science* **365**, 264–267 (2019).
34. S. D. Hann, T. H. Niepa, K. J. Stebe, D. Lee, One-step generation of cell-encapsulating compartments via polyelectrolyte complexation in an aqueous two phase system. *ACS Appl. Mater. Interfaces* **8**, 25603–25611 (2016).
35. N. Tompkins *et al.*, Testing turing's theory of morphogenesis in chemical cells. *Proc. Natl. Acad. Sci. U.S.A.* **111**, 4397–4402 (2014).